Do Adriatic Bora winds impact Venice?

Rizwan Qayyum (rizwan.qayyum@ufl.edu)
University of Florida College of Engineering: University of Florida Herbert Wertheim College of Engineering https://orcid.org/0000-0002-9415-7978

Lorenzo Melito
Polytechnic University of Marche Department of Architecture Buildings and Structures: Universita Politecnica delle Marche Dipartimento di Ingegneria Civile Edile e Architettura

Joseph Calantoni
US Naval Research Laboratory

Maurizio Brocchini
Polytechnic University of Marche Department of Architecture Buildings and Structures: Universita Politecnica delle Marche Dipartimento di Ingegneria Civile Edile e Architettura

Alex Sheremet
University of Florida College of Engineering: University of Florida Herbert Wertheim College of Engineering

Research Article

Keywords: Bora wind forcing, Transversal Adriatic seiche, Period ≈ O(100 min), Analytical model

Posted Date: March 11th, 2022

DOI: https://doi.org/10.21203/rs.3.rs-1428523/v1

Do Adriatic Bora winds impact Venice?

Rizwan Qayyum[1*], Lorenzo Melito[2], Joseph Calantoni[3], Maurizio Brocchini[2] and Alex Sheremet[1]

[1*]Engineering School of Sustainable Infrastructure and Environment, University of Florida, Gainesville, FL, USA.
[2]Department of Engineering, Civil, Construction and Architecture, Marche Polytechnic University, Ancona, Italy.
[3]U.S. Naval Research Labortary, Stennis Space Center, MS, USA.

*Corresponding author(s). E-mail(s): rizwan.qayyum@ufl.edu;
Contributing authors: l.melito@pm.univpm.it;
joe.calantoni@nrlssc.navy.mil; m.brocchini@univpm.it;
alex.sheremet@essie.ufl.edu;

Abstract

The Jan. 2014 Adriatic Bora storm produced a measurable impact in north Adriatic, where tidal gauges recorded 5-cm sea-level fluctuations with a characteristic period of 100 min. Given the sensitivity of Venice flooding to sea-level perturbations and the localized, basin-transversal jet structure of the Bora winds, the observations are both significant and surprising. We investigate the event based on field observations off the Senigallia coast, Italy, and use simple linear analytical and numerical models. The model suggests that the oscillations observed are a mixture of edge-waves and seiches with a significant basin-transversal component, generated during the relaxation of Bora wind setup. The spatial structure of seiches explains the surprising basin-longitudinal reach of Bora storm. Despite the model simplicity, simulations results are consistent with sea-level measurements. The study suggests that Bora winds may have an impact on Venice and its surroundings and deserve more consistent monitoring and more accurate modeling.

Keywords: Bora wind forcing, Transversal Adriatic seiche, Period $\approx$ O(100 min), Analytical model

1 Introduction

In their study of resonant amplification of tides by longitudinal seiches in the northern Adriatic, Medvedev et al (2020) note the interesting fact that "*coincident storm surge and high tide* can double the flooded area of Venice" (our emphasis). They give the example of the Nov. 2019 flood, caused by the coincidence of lower high water ($\approx$ 187 cm) and a 30-cm storm surge; 80% of Venice flooded, with damages estimated at 1.1 B €. Without the additional 30-cm surge, the damage would have been 20-25% less (Medvedev et al, 2020; Ferrarin et al, 2021).

As main contributors to Venice flooding, the basin-longitudinal seiches (fundamental period 21.5 hr) have been extensively studied (Vercelli, 1941; Stravisi, 1972; Poretti, 1974; Manca et al, 1974). However, the seemingly disproportionate effect of small sea-level perturbations raises the question of whether shorter fluctuations, in the order of hours, might have significant effects. Such fluctuations, with heights in the order of 20 cm, are frequent in winter (Figure 1(a)) and persist for several days, long enough to overlap with high tides. While many such events (e.g., A and B in Figure 1(a)) are associated with longitudinal Adriatic surges, the Jan. 25th event (C in Figure 1(a)) stands out as a basin-transversal phenomenon, caused by a Bora storm (Figure 1(b)). Given the specific structure of Bora winds (Signell et al, 2010), with highly localized, fixed-positioned jets that mostly impact the Ancona-Ortona segment of the Italian shore (Figure 1(b)), it is surprising to detect measurable effects as far north as Venice.

Here, we investigate the nature and generation mechanism of the Jan. 25th, 2014 oscillations. The opportunity for this study is provided by the EsCoSed field experiment (Brocchini et al, 2017), which captured in detail the Jan. 2014 Bora storm. The experiment deployed an array of hydrodynamic sensors in a cross-shore transect covering the mouth of the Misa river and approx. 800 m in the nearshore (Figure 2(a)). Instruments included high-resolution velocity profilers, as well as pressure and sediment concentration sensors (for details of the suite of instruments and the experiment schedule, see Brocchini et al (2017)). The analysis presented here focuses on the measurements collected by the Nortek Aquadopp Profiler, deployed at the mouth of the Misa River (QR3, Figure 2(a)).

2 Field observations and Methods

At Senigallia, the storm generated a 0.35-m surge (Figure 2(c) and (e)) and energetic waves of 10-s peak period and 3-m significant height (Brocchini et al, 2017). In the two relatively calm days following, the QR3 sensor recorded persistent low-frequency oscillations of sea level and flow velocity, with sea-level periods between 20 min and 120 min, and amplitudes in the order of 10 cm and 10-20 cm/s (Figure 2(b) and (d); alongshore velocities $\approx$ 2 cm/s). The oscillations were in phase through the entire cross-shore array of instruments (QR1 to QS3, Figure 2(a)). Spectral estimates of the pressure, cross- and

along-shore velocity during this period (Figure 2(f)) exhibit discrete peaks at frequencies $\approx nf_0$, with $n = 1, 2, \cdots$, and $f_0 = 0.01$ min^{-1}.

The origin of these oscillations is not clear. For example, similar low-frequency observed at the Port of Rotterdam, Netherlands (De Jong and Battjes, 2004), were likely generated through Proudman resonance (Proudman, 1929) by convection cells moving over the North Sea. However, this mechanism seems inconsistent with the persistence (2 days) of the oscillations, the Adriatic scale, and its surrounding orography. The characteristic time scale of the oscillations and the structure of their power spectrum suggests seiche modes with a significant basin-transversal component.

Figure 2 shows analyses of the measurements at the Misa River mouth (sensor QR3, Nortek ADV; see Fig 1a). To estimate the power spectra of velocity components and pressure (Figure 2(f)), downsampled time series (from 2 Hz to a 1 min^{-1}) covering the post-Bora time segment considered here, Jan. 25th, 20:00 hr to Jan. 29th, 12:00 hr local time (local time is UTC+1) was divided into 6 segments of 1024 points (≈17 hr) with 50% overlap, Fourier transformed and averaged (Welch method, (Welch, 1967)). While 6 degrees of freedom is generally considered low for a spectral estimate of free surface elevation, the time average is used here mostly as a smoothing device to highlight the position of the spectral peaks.

Sea-level time series recorded by tidal gauges at Venice, and Ortona have a coarse sampling interval of 10 min. The time series of envelope heights shown in Figure 1(a) were obtained by applying a moving mean band-pass filter that suppressed the signal outside the frequency band of [1/120, 1/20] min^{-1}.

In Section 3, seiche modes for the trapezoidal cross-shore profile are calculated by the shooting technique (Press et al, 2007), while edge-wave modes are calculated using the well studied free Stokes edge-waves on a plane beach (Kurkin and Pelinovsky, 2002).

3 Mathematical model and simulations

The nature of the observed oscillations is investigated here using a simplified approach that combines analytical and numerical methods, applied to a simplified geometric representation of the Adriatic basin. Adriatic bathymetry is quite complex. The northern transversal profiles are roughly trapezoidal, sloping on the eastern shore (e.g. Figure 3(a)), and become more symmetric in the southern half. In the longitudinal direction, the northern half does not exceed 200 m depth, whereas the South Adriatic Pit is over 1,200 m deep. However, due to its roughly rectangular shape, the basin bathymetry in longitudinal direction has often been approximated as a prism in past analytical studies of Adriatic seiches (e.g. Defant (1961); Bajc (1972) with $h \approx 240$ m, reviewed in Franco et al (1982); Vilibić et al (1998); Leder and Orlic (2004)).

3.1 Adriatic sea bathymetry and representations

Following Defant (1961) and Bajc (1972), we consider several prismatic approximations of the Adriatic bathymetry. The planar shape of the basin is represented as rectangles with different lengths depending on the type of southern boundary (Figure 3(a)). The bathymetry is approximated as cylindrical, i.e., $h = h(x)$, with $h(0) = h(W) = 0$, where h is the depth and x and y axes are transversal and longitudinal, respectively, with either a flat bottom (h =constant), or trapezoidal transversal profile (Figure 3(d); see also Tab. 1 for details).

The complexity of the Adriatic bathymetry allows for no obvious choice for the maximum depth $h_{\max}$ of the bathymetry. To overcome this problem, we conducted a preliminary numerical search (not a systematic optimization) for $h_{\max}$ values that returned seiche frequencies distributed like nf_0, with $n = 1, 2, \cdots$, and $f_0 = 0.01$ min^{-1}, similar to observations. The distribution of the eigenfrequencies for the selected values of $h_{\max}$ is shown in panels of top row in Figure 4.

3.2 Simplified mathematical model

Seiche hydrodynamics is represented here using the linearized shallow water equations

$$u_t + g\eta_x = 0,\ v_t + g\eta_y = 0,\ \eta_t + (uh)_x + (vh)_y = 0, \tag{1}$$

where x and y are coordinates along the transversal and longitudinal axes of the Adriatic (Figure 3(a)); h is the local still-water depth; η is the free surface elevation; u and v are velocity components along the x and y axes and the subscripts give partial derivatives. It can be shown that for seiche time scales of interest here, the Coriolis effect may be neglected in the leading order. Nonlinear effects are negligible because the characteristic amplitude of the oscillations O(cm) is several orders of magnitude smaller than the characteristic wavelength O(km).

At a closed side of the rectangle, solutions of Eq. (1) satisfy the boundary condition $\vec{u} \cdot \vec{n} \mid_S = 0$,where $\vec{u} = (u, v)$ is the flow velocity vector and $\mathbf{n}$ is the unit vector normal to the closed boundary S pointing outward. If the side S is open, the boundary condition is $\eta|_S = 0$.

For a sloping cylindrical bathymetry $h(x)$, two tranversally distinct families of solutions are possible: a) seiches, which have an oscillatory structure, and span the entire width of the basin, and b) edge-waves, which exhibit cross-shore turning point where they switch between oscillatory and exponential behavior. Because we are interested here in oscillations detectable on the western Adriatic shore only, we will consider edge-wave modes, trapped on the western slope. Hence, western slope is treated as mildly sloping while eastern slope is vertical in trapezoidal representation (see Figure 3(d)).

The linear shallow water seiche/edge-wave problem is well understood (Kirby et al, 2007; Rabinovich, 2010; LeBlond and Mysak, 1981). Our

bathymetric choices allow for using the method of separation of variables

$$\begin{bmatrix} \eta \\ u \\ v \end{bmatrix} = a \begin{bmatrix} H\,(x) \\ U(x) \\ V(x) \end{bmatrix} Y(y)T(t) \tag{2}$$

where a is the modal amplitude (constant), and H,U,V, Y, and T are functions that describe the spatial and temporal structure of the oscillations. The Y functions are orthonormal, in the sense that $\frac{1}{L}\int_0^{2L} Y_n Y_{\tilde{n}} dy = \delta_{n\tilde{n}}$. For a basin closed at both ends in the y direction

$$\begin{bmatrix} \eta \\ u \\ v \end{bmatrix} = a \begin{bmatrix} H(x)\cos\left(k_n y\right)\cos\left(\omega t\right) \\ -\frac{g}{\omega}H_x(x)\cos\left(k_n y\right)\sin\left(\omega t\right) \\ \frac{gk}{\omega}H(x)\sin\left(k_n y\right)\sin\left(\omega t\right) \end{bmatrix}, \tag{3}$$

where $k_n = \frac{n\pi}{L}$, $n = 1, 2, \cdots$. For a basin that has an open side at the southern end (e.g., red rectangle in Figure 3), the solution is

$$\begin{bmatrix} \eta \\ u \\ v \end{bmatrix} = a \begin{bmatrix} H(x)\sin\left(k_n y\right)\sin\left(\omega t\right) \\ \frac{g}{\omega}H_x(x)\sin\left(k_n y\right)\cos\left(\omega t\right) \\ \frac{gk}{\omega}H(x)\cos\left(k_n y\right)\cos\left(\omega t\right) \end{bmatrix} \tag{4}$$

with $k_n = \frac{(2n-1)\pi}{2L}$, $n = 1, 2, \cdots$. In both cases, the radian frequency of the oscillation $\omega(k_n)$ is obtained as the eigenvalue of the singular Sturm-Liouville problem

$$\left(c^2 H_x\right)_x + \left(\omega^2 - k_n^2 c^2\right) H = 0, \tag{5}$$

completed by boundary conditions at $x = 0$ and $x = W$. Eq. (5) is a general equation for the cross-shore structure of the Adriatic oscillations, satisfied by both seiche and edge-wave modes.

Changing the function H to $G(x) = H(x)\exp\frac{1}{2}\int^x \frac{dh}{h}$ brings Eq. (5) to the form

$$G_{xx} + R(x)G = 0, \quad R = \frac{\omega^2}{gh} - k_n^2 - \frac{1}{4}\frac{2h_{xx}h - h_x^2}{h^2}. \tag{6}$$

The turning points of G (and H) are the roots of equation $R = 0$. Seiches are solutions of Eq. (5) that correspond to $R > 0$ over the entire domain. If the bathymetric profile $h(x)$ is mildly sloping, the derivatives of h in Eq. (6) may be provisionally neglected, yielding approximate turning point positions as roots of equation

$$\omega^2 - k_n^2 c^2 = 0. \tag{7}$$

In Eq. (7), turning points represent depths for which the alongshore component of the modal phase speed equals $c = \sqrt{gh}$. Because $\omega^2 - c^2 k_n^2 \to \omega^2 > 0$ as $h \to 0$, the existence of a turning point requires that $\omega^2 - c_{\max}^2 k_n^2 < 0$ at the deepest point $h_{\max} = \max(h)$ of the transversal bathymetric profile. Using this approximation, the solutions of Eq. (5) are separated into the seiches, satisfying $\omega^2 - c_{\max}^2 k_n^2 > 0$, and edge-waves, satisfying $\omega^2 - c_{\max}^2 k_n^2 < 0$.

Seiche solutions have oscillatory behavior in the entire domain $[0, W]$, and their transversal structure satisfies zero-flux boundary conditions at the lateral boundaries

$$u(x = 0, y, t) = u(x = W, y, t) = 0, \text{ or } H_x \mid_{0,W} = 0. \tag{8}$$

For a flat bottom $h = h_0$, Eq. (5) takes the simple form$H_{xx} + k_m^2 H = 0$, where $k_m^2 = \frac{\omega_{n,m}^2}{gh} - k_n^2$ is the wave number component in the transversal direction. Imposing the boundary conditions (8) obtains

$$\frac{\omega_{n,m}^2}{gh} = k_m^2 + k_n^2, \quad k_m = \frac{m\pi}{W}, \; m = 0, 1, 2, \cdots, \tag{9}$$

with H given by $H_m = \cos k_m x$. The functions H_m are orthonormal, i.e., $\frac{1}{W}\int_0^{2W} H_m H_{\tilde{m}} dx = \delta_{m\tilde{m}}$.

For the trapezoidal bathymetry, we obtain seiche modes solution with the shooting technique. Using substitution $G = H_x$, Eq. (5) is reduced to an initial value problem with initial value $[H, G](x = 0) = [1, 0]$, and value of $[H, G](x = W)$ is approximated, using shallow water approximation of the eigenvalue, $c = \sqrt{gh_{max}}$. In subsequent iterations, value of c is modified so that other side boundary condition $G(x = W) = 0$ is attained to reasonable accuracy. For the edge-wave modes, plane beach solution (Kurkin and Pelinovsky, 2002) is used, given by

$$H_m = e^{(-k_n x)} L_m (2k_n x),$$

where L_m is the Laguerre polynomial. One can also easily verify the edge-wave and seiche modes are orthogonal. The general solution for a trapezoidal bathymetry may therefore be written as

$$\eta = \sum_{n,m} a_{n,m}^S \eta_{n,m}^S + \sum_{n,m} a_{n,m}^E \eta_{n,m}^E, \tag{10}$$

where superscripts S and E denoting seiche and edge-wave modes. The modal amplitudes $a_{n,m}^{S,E}$ are obtained by projecting the initial condition $\eta_0 = \eta(x, y, t = 0)$ on the basis $\{\eta_{n,m}^S, \eta_{n,m}^E\}$,

$$a_{n_x n_y}^{S,E} = \frac{1}{LW} \int_0^{2L} \int_0^{2W} \left(Y_{n_y} H_{n_x}^{S,E} \eta_0\right) dxdy. \tag{11}$$

3.3 Numerical simulation

We hypothesize that the Bora winds create a localized wind setup in the northwestern Adriatic and that the observations represent the relaxation process after the Bora forcing is removed. This hypothesis is tested here in two steps.

Step 1 solves Eq. (5) with the selected boundary conditions for the full set of eigenfrequencies and eigenfunctions, providing the orthonormal basis for the decomposition in Eq. 10. For the trapezoidal transversal profile, the solutions are computed numerically, using the shooting method described in Section 2. Step 2 computes the amplitude spectrum of a candidate wind setup model (Eq. (11)) by projecting its free-surface shape $\eta_0(x, y)$ on the eigenfunction basis generated at step 1. Both steps are iterative. At step 1, the iterations are used to select an "adequate" maximal depth $h_{\max}$ for each profile, as explained in Section 3. At step 2, the exact shape of the initial setup is unknown; we represent the initial perturbation as a Gaussian

$$\eta(x, y, t = 0) = Ae^{-\left(\frac{x}{\alpha W}\right)^2 - \left(\frac{y-y_0}{\beta L}\right)^2}, \tag{12}$$

with the peak height of 0.35 m located at the approximate Senigallia position, 150 km south of the northern Adriatic boundary. The width factors α and β given in Table 1, are selected to yield spectra which approximately match the observed spectra. The selected value of the width factor β is consistent with the longitudinal impact of Bora jets on western shore e.g see Figure 1.

To demonstrate the features of the solution, the model is used to generate 60-hours time series of the setup relaxation for all the cases at mock representation of Senigallia (red solid circle; Figure (3)(a)), and the time series are analyzed using the same procedure that was applied to the observations. Figure 4 shows a summary of the simulations. The upper row of panels show the distribution of eigenfrequencies for seiche and edge-wave modes. The middle and lower rows of panels compare the simulations to the observations. The columns of panels correspond to the four bathymetrical approximations used (Figure 3 and Table 1). For the trapezoidal profile, the normalized amplitude spectrum shown in Figure (5)(a) highlights the relative contribution of different modes. Reconstructing the (simulated) free-surface elevation at any point of the Adriatic basin (in the simplified bathymetry) is straightforward. Panels (b), (c) and (d) of Figure 5 show an example of amplitudes of oscillations and spectrum at an arbitrary point, P in the north Adriatic near the northwest corner of the bathymetry, located in a longitudinal direction away from perturbation (shown as black arrow in Figure 3). The simulated wind setup produces oscillations in the order of 5 cm height (see Figure 5(b)), consistent with the magnitude of observations in north Adriatic (Figure 1(a)).

Conclusion

The hydrodynamic model presented here uses a highly simplified bathymetry, and does not account for Earth rotation, stratification, currents, and nonlinearity. These processes were assumed to have a higher-order contribution to the oscillations, but the validity of this assumption was not investigated here in any detail. Despite its simplicity, the model supports the hypothesis that

the oscillations observed are a mixture of edge-waves and seiches with a significant transversal component, generated during the relaxation of the Bora wind setup. The model suggests that excited seiche and edge-wave modes have a strong longitudinal component, which explains why effects should be detectable throughout the Adriatic. The results suggest that Bora winds may have an impact on Venice flooding, and deserve more consistent monitoring and more accurate modeling.

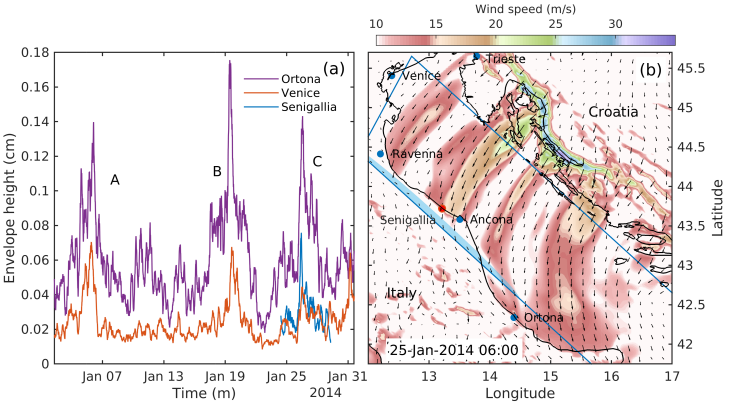

Fig. 1 Summary of effects and structure of the Jan. 2014 Bora storm. a) Smoothed height of sea level perturbations in the frequency band $[1/120, 1/20]$ min^{-1} (Italian National Tidegauge Network, ISPRA

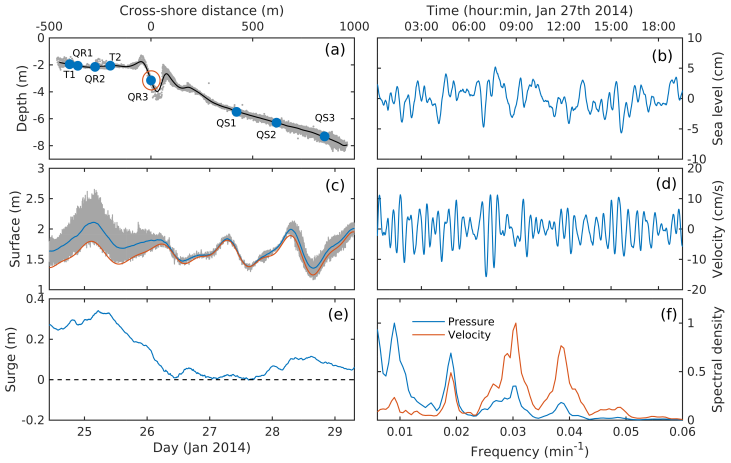

Fig. 2 Observations of the Bora storm at Senigallia, Italy. a) Bathymetric profile and instrument locations (for details see Brocchini et al (2017)). The data discussed in this study was provided by the QR3 instrument (red circle) deployed at the Misa River mouth (Nortek Vector ADV, sampling at 2 Hz in bursts of 40 min located 0.54 m above bed in 3.15 m deep water. b,d) Example time series of the sea level and cross-shore velocity oscillations recorded at QR3. c) Sea level observations (gray), mean sea level (blue line), and tide level at QR3. e) Storm surge, calculated as the difference between mean water level and tidal level. f) Normalized power spectra of sea-level and cross-shore velocity oscillations.

254

Table 1 Parameters used in simulations for the flat bottom and trapezoidal transects. "Open" and "Closed" describe the southern boundary condition: either allowing free flow through, or not; L and W are the length of the longitudinal and transversal sides of the rectangle; h is the depth.

			Flat				Trapezoidal			
Basin	L(km)	W(km)	Type	h(m)	α	β	h(m)	Slope	α	β
Closed	750	150	LC	235	0.13	0.35	380	6.3×10^{-3}	0.035	0.17
Open	750	150	LO	242	0.13	0.35				
Open	500	150	SO	239	0.13	0.35				

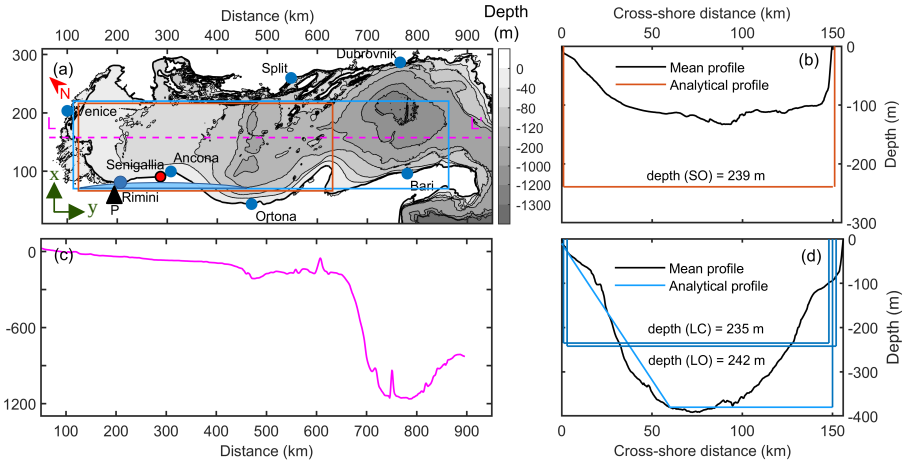

Fig. 3 Adriatic bathymetry and bathymetric models. a) Adriatic bathymetry with two rectangular models with dimensions 750 km × 150 km (blue rectangle) and 500 km × 150 km (red rectangle). The blue half-ellipse represents elevations > 5 cm, corresponding to the surge used in simulations. The black arrow marks an arbitrary location in the north Adriatic (also see Figure (5)(b), (c) and (d)). b) Mean transversal bathymetric profile (black) for red rectangle in panel (a); flat bottom profile (red) used in simulations. c) Bathymetric profile of the Adriatic basin along section $L - L'$ in panel (a). d) Mean transversal bathymetric profile (black) for the blue rectangle in panel (a); flat and trapezoidal profiles (blue) used in simulations. The mean bathymetric profiles in panels Figure 3(b) and (d) were computed by first stretching all basin-transversal profiles to the same width W and then averaging in the longitudinal direction. Table 1 provides parameters for each representative profile shown in panels (b) and (d).

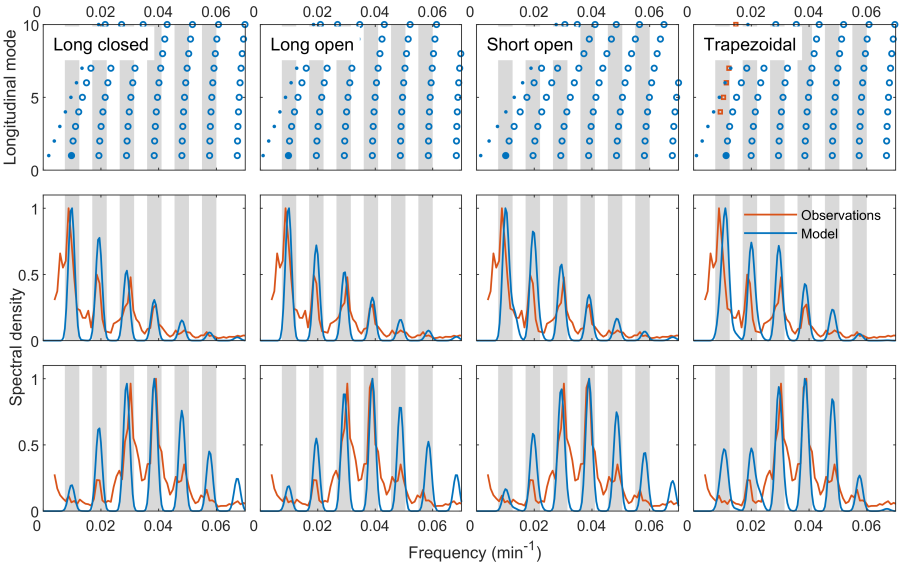

Fig. 4 Eigenfrequencies for the four cross-shore profiles (shown in Figure 3(b) , (d)). Top row: dispersion relation. Mode with $n > 0$ (circles) exhibit basin-transversal oscillations. Modes with $n = 0$ (dots) are purely basin-longitudinal modes. For the profiles selected for simulations, the frequency of mode $(n, m) = (1, 1)$ (blue disk) is 0.01 min $^{-1}$, where m is basin-longitudinal mode number. Middle and bottom rows: comparison of simulated (blue) and observed (red) spectra of pressure and cross-shore velocity. Gray rectangles mark the approximate location of the peaks of the observed spectra.

256

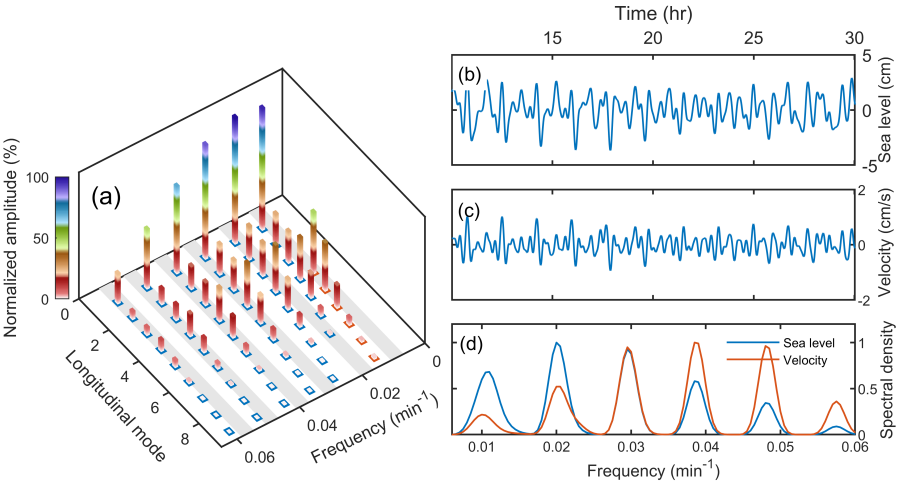

Fig. 5 Numerical results using trapezoidal bathymetry of a) amplitudes of the modal constituents of the simulation results at Senigallia (marked by red solid circle in Figure 3(a)); amplitudes normalized with maximum amplitude and expressed in percentage; blue pedestals mark seiche modes; red pedestals mark edge-wave modes. b) Sea-level, c) cross-shore velocity and d) power spectra of the oscillations at an arbitrary location, P in north Adriatic (marked by black arrow in Figure 3(a)).

Acknowledgments. The work of Mr. Qayyum and Prof. Sheremet was supported by NSFGOE-NERC grant No. 1737274, and NRL cooperative agreement award No. N00173 -21-2-C900. Prof. Sheremet is grateful for the support and advice of Prof. V.I. Shrira, Keele University, UK.

The work of Prof. Brocchini's contribution was supported by the Office of Naval Research Global (UK) MORSE Project (Research Grant Number N62909-17-1-2148), the MIUR PRIN 2017 Project, Italy "FUNdamentals of BREAKing wave-induced boundary dynamics – FUNBREAK" (Grant Number 20172B7MY9) and, Parco Nazionale del Circeo (Lazio Region, Italy).

Declarations

- **Funding** Already covered in acknowledgments section.
- **Conflict of interest** There is no conflict of interest.
- **Ethics approval** Not applicable
- **Consent to participate** All authors designed the study, collected data, wrote the manuscript and revised it.
- **Consent for publication** All authors agree to publish this manuscript.
- **Availability of data and materials**The data is available through (Brocchini et al, 2017) (https://doi.org/10.1016/j.margeo.2016.12.005).
- **Code availability** Not applicable
- **Authors' contributions** All authors designed the study, collected data, wrote the manuscript and revised it.

References

Bajc D (1972) Seiches in the Adriatic Sea: A theoretical approach. Boll di GeoJs Teor Appl 14:25–33

Brocchini M, Calantoni J, Postacchini M, et al (2017) Comparison between the Wintertime and Summertime Dynamics of the Misa River Estuary. Marine Geology 385:27–40. https://doi.org/10.1016/j.margeo.2016.12.005

De Jong MPC, Battjes JA (2004) Low-frequency Sea Waves Generated by Atmospheric Convection Cells. Journal of Geophysical Research: Oceans 109(C1). https://doi.org/10.1029/2003JC001931

Defant A (1961) Physical oceanography, vol 1. Pergamon

Ferrarin C, Bajo M, Benetazzo A, et al (2021) Local and Large-scale Controls of the Exceptional Venice Floods of November 2019. Progress in Oceanography p 102628. https://doi.org/10.1016/j.pocean.2021.102628

Franco P, Jeftic L, Rizzoli PM, et al (1982) Descriptive model of the Northern Adriatic. Oceanologica Acta 3:379–389. URL https://archimer.ifremer.fr/doc/00121/23176/21021.pdf

Kirby JT, Özkan Haller HT, Haller MC (2007) Seiching in a large wave flume. In: Coastal Engineering 2006: (In 5 Volumes). World Scientific, chap 1159-1171, https://doi.org/10.1142/9789812709554_0099

Kurkin A, Pelinovsky E (2002) Focusing of Edge Waves above a Sloping Beach. European Journal of Mechanics-B/Fluids 21(5):561–577. https://doi.org/10.1016/S0997-7546(02)01201-3

LeBlond P, Mysak L (1981) Waves in the Ocean. Elsevier

Leder N, Orlic M (2004) Fundamental Adriatic seiche recorded by current meters. In: Annales Geophysicae, Copernicus GmbH, pp 51–60, https://doi.org/10.5194/angeo-22-1449-2004

Manca B, Mosetti F, Zennaro P (1974) Analisi spettrale delle sesse dell'Adriatico. Bolletino di Geofisica Teorica ed Applicata 16

Medvedev IP, Vilibić I, Rabinovich AB (2020) Tidal resonance in the Adriatic Sea: Observational evidence. Journal of Geophysical Research: Oceans 125(8). https://doi.org/10.1029/2020JC016168

Poretti G (1974) Computation of the free oscillations of the Adriatic with the hydrodynamical numerical method. Atti dell'Accademia Nazionale del Lincei, Quad N 206:153–157

Press WH, Teukolsky SA, Vetterling WT, et al (2007) Numerical Recipes 3rd Edition: The Art of Scientific Computing. Cambridge university press, URL https://personal.sron.nl/~kuiper/hea_inst11/exercise-2/Varia/Numerical-Recipes/f0-0.pdf

Proudman J (1929) The Effects on the Sea of Changes in Atmospheric Pressure. Geophysical Supplements to the Monthly Notices of the Royal Astronomical Society 2(4):197–209. https://doi.org/10.1111/j.1365-246X.1929.tb05408.x

Rabinovich AB (2010) Seiches and harbor oscillations. In: Handbook of coastal and ocean engineering. World Scientific, p 193–236, https://doi.org/10.1142/9789812819307_0009

Signell RP, Chiggiato J, Horstmann J, et al (2010) High-resolution mapping of Bora winds in the northern Adriatic Sea using synthetic aperture radar. Journal of Geophysical Research: Oceans 115(C4). https://doi.org/10.1029/2009JC005524

Stravisi F (1972) A numerical experiment on wind effects in the Adriatic Sea. Accademia Nazionale dei Lincei, Rendiconti 8/53,2

Vercelli F (1941) Le maree e le sesse nel porto di Zara. La Ricerca Scientifica 12(1)

Vilibić I, Leder N, Smirćić A (1998) Forced and free response of the Adriatic sea level. Il Nuovo Cimento C (4):439–452. URL http://eprints.bice.rm.cnr.it/12834/

Welch P (1967) The use of Fast Fourier Transform for the estimation of Power Spectra: A Method Based on Time Averaging over short, modified Periodograms. IEEE Transactions on audio and electroacoustics 15(2):70–73